Наносистеми, наноматеріали, нанотехнології
Nanosistemi, Nanomateriali, Nanotehnologii
2026, т. 24, № 1, сс. 225–240
https://doi.org/10.15407/nnn.24.01.0225

PACS numbers: 68.37.Hk, 68.37.Vj, 78.20.Ci, 78.40.Ha, 78.67.Uh, 81.07.Gf, 81.15.Gh

Effect of Aluminium Doping on the Characteristics of One-Dimensional Zinc-Oxide Nanowires Grown by Atmospheric Pressure Chemical Vapour Deposition

Zahra Mohammed Saeed[1], Samir Mahmmod Ahmad[2], and Yasir Hussein Mohammed[3]

[1]*Polytechnic College Mosul,*
Department of Electrical Techniques,
Northern Technical University,
41002 Mosul, Iraq
[2]*College of Science,*
Department of Physics,
University of Mosul,
41002 Mosul, Iraq
[3]*College of Education for Pure Science,*
Department of Physics,
University of Mosul,
41002 Mosul, Iraq

The atmospheric-pressure chemical vapour deposition (APCVD) technique is used to grow ZnO nanowires (NWs) on glass substrates. The effect of different doping ratios (0, 2, 4, and 6 wt.%) of aluminium on the structure, morphological and optical properties of the ZnO:Al nanowires is studied. The optical, structural, and morphological results were evaluated using ultraviolet–visible (UV–Vis) spectroscopy, x-ray diffraction (XRD), and field emission scanning electron microscopy (FE–SEM) with energy dispersive x-ray (EDX) spectroscopy. Optical results indicate that, with the increase of aluminium doping, the interatomic distance in the crystal lattice is decreased, and the energy gap is shifted to redshift. The doping with aluminium improves the crystallinity of the network. Morphological observations indicate that, when measuring the diameters of ZnO nanowires, the diameter of the aluminium-doped ZnO nanowires increases with increasing doping ratio. The surface of the ZnO nanowires also contains Al atoms, and EDX spectroscopy supports this finding. Our current research may serve the development of future nanooptical devices.

Для вирощування нанодротів (НД) ZnO на скляних підкладинках було використано метод хемічного осадження з парової фази (APCVD) за ат-

мосферного тиску. Було досліджено вплив різних ступенів леґування (0, 2, 4, 6 мас.%) алюмінієм на структурні, морфологічні й оптичні властивості нанодротів ZnO:Al. Оптичні, структурні та морфологічні результати оцінювали за допомогою ультрафіолетової й оптичної (UV–Vis) спектроскопії, рентґенівської дифракції (XRD) та польової емісійної сканувальної електронної мікроскопії (FE–SEM) з енергодисперсійною рентґенівською (EDX) спектроскопією. Оптичні результати показали, що зі збільшенням леґування алюмінієм міжатомова віддаль у кристалічній ґратниці зменшується, а енергетична щілина зміщується в бік довших хвиль. Леґування алюмінієм поліпшило кристалічність структурної мережі. Морфологічні спостереження показали, що з мірянням діяметрів нанодротів ZnO діяметер леґованих алюмінієм нанодротів ZnO збільшувався зі збільшенням ступеня леґування. Поверхня нанодротів ZnO також містила атоми Al, а EDX-спектроскопія підтвердила цей висновок. Наші поточні дослідження можуть сприяти розробці майбутніх нанооптичних пристроїв.

Key words: atmospheric-pressure chemical vapour deposition, ZnO nanowires, band gap, doping with Al, vapour–solid process.

Ключові слова: хемічне осадження з парової фази за атмосферного тиску, ZnO нанодроти, заборонена зона, Al-леґування, парофазний процес.

(Received 15 August, 2024; in revised form, 30 September, 2025)

1. INTRODUCTION

ZnO strong exciton-binding energy of 60 meV at room temperature, wide band gap of 3.37 eV, strong radiation tolerance, high thermal conductivity, high electron mobility, and high breakdown electric-field strength are appropriate for optoelectronics, laser technology, and electronics applications [1, 2]. There are various structural arrangements of ZnO nanomaterials [3] such as nanotubes [4], nanowires (NWs) [5], nanobelts [6], nanorods [7], nanoribbons [8], and nanocables [9]. Numerous ZnO nanowires distinguish from the rest of the configurations with the large surface-to-volume ratio, which gives a large active area, the high electron mobility, and transparency, are worthy for the electron-transport layer, which is beneficial for UV lasers [10], light-emitting diodes [11], solar cells [12], nanogenerators [13], gas sensors [14], photodetectors [15], and photocatalysts [16].

Aluminium (Al) is a cheap and abundant element; hence, Al:ZnO could be a good replacement for indium–tin oxide films, which are commonly used in solar energy systems [17]. It has been believed that adding dopants Ga, In, Li, Cu, Al, *etc.* is one of the easiest ways to control the nanostructures produced by chemical vapour deposition [18]. It should be mentioned that the band-gap energy of

ZnO is lowered by Cd, Ti, and Al, but raised by Li and Mg, for example [19]. Increasing ZnO electrical conductivity is the primary objective of Al doping. The doping concentration primarily dictates where the Al atom is located inside the ZnO lattice; at concentrations below 2%, it occupies the Zn site, while, at concentrations above 2%, it occupies the interstitial site. The concentration of free carriers increases, when Al^{3+} is used in place of Zn^{2+} [20].

Previous research investigated the effects of Al doping on properties of ZnO nanowires; however, a detailed analysis is still required to ascertain the effects of Al-doping concentration on ZnO [21–23]. Many deposition methods like sputtering [24], pulsed laser deposition [25], chemical vapour deposition, spray pyrolysis [26], and sol–gel processing [27] ways have been adduced to produce Al:ZnO nanowires. The method used in this paper, the chemical vapour deposition (CVD) method, for growing ZnO NWs does not require complex equipment or high vacuum and can be adapted to many practical variations. Its flexibility, thus, allows for many composition and location changes during deposition. This results in high-quality materials, *i.e.*, with excellent homogeneity and purity of the fabricated material, step coverage, and adhesion, high productivity, *etc.* [28]. In this work, pure ZnO and Al:ZnO nanostructures were produced *via* the chemical vapour deposition approach. It examined the relationship between Al concentration and both the growth of morphology and the tuning of the optical band gap. It was demonstrated that the evolution of surface form and optical properties was related to the Al content in the Al:ZnO nanostructures.

2. EXPERIMENTAL DETAILS

Initially, the glass substrates of 10×10 mm was ultrasonically cleaned in acetone, ethanol, and deionized water (D_I) for ten minutes in each solution to eliminate impurities. Then, high-purity zinc acetate dihydrate 99.97% $Zn(CH_3COO)_2{\cdot}2H_2O$ was used to produce zinc vapour, while aluminium nitrate $Al(No_3)_3{\cdot}9H_2O$ was used to dope aluminium with 0, 2, 4, and 6 wt.% for 1*D* ZnO NWs growth *via* a dual-zone APCVD method at growth temperature of 600°C. Growing low-dimensional nanomaterials *via* vapour-transport deposition within the horizontal tube furnace are widely used [29]. A thorough explanation of the APCVD system was provided in another place [30].

The temperature of growth was raised by 10°C/min. The substrate and activator were weighed according to the weight ratios listed in Table 1 and placed in an alumina boat (5 cm) away from the flat steel substrate holder; after inserting them into the deposi-

TABLE 1. The proportions of doping.

Fixed weight	Fixed ratio	Weight of doping material	Weight of base material	The mixture weight remains constant
Zn acetate, g	Percentage	Al nitrate, g $\equiv x$	Zn acetate, g $\equiv (1-x)$	Total, g
0.8	0%	0.016	0.784	0.8
0.8	2%	0.032	0.764	0.8
0.8	4%	0.048	0.752	0.8
0.8	6%	0.064	0.736	0.8

tion reactor, the quartz tube was tightly closed to prevent any leakage out of the system. 1*D* ZnO NWs were synthesized for 10 min at evaporation temperature of 600°C using O_2 gas applied at a flow rate of 25 cm^3/min. The temperature of growth was raised by 10°C/min. To regulate precisely the flow rate, a mass flow controller (MFC) was used.

Then, without an oxygen atmosphere, the samples were annealed for three hours at a constant temperature of 600°C. Every other parameter related to the growth was maintained at a constant level and closely monitored. Finally, after the annealing time was over and the furnace was switched off, and once it gradually cooled down to room temperature, the samples were taken out from the reactor and analysed. It should be noticed that the substrates darkened (took on a brown tinge). A UV–Vis spectroscopy (UV-1800 Shimadzu, Japan) was utilized to measure the optical transmittance (*T*) and absorbance (*Abs*) spectra of the grown materials ZnO NWs/glass in the 360–1000 nm wavelength range, with bare glass serving as a reference. Using an x-ray diffractometer (Malvern PANalytical-Aeris) with CuK_α ($\lambda = 1.5406$ Å) radiation operating at 40 kV and 30 mA, the orientation and crystal structure of the grown samples (ZnO NWs/glass) were confirmed. The samples were scanned in the range of 25–75° with an angle step size of 0.011°. FE–SEM equipped with EDX spectroscopy was inviting to obtain surface and cross-sectional images and settle the chemical composition of the grown samples.

3. RESULTS AND DISCUSSION

UV–Vis spectroscopy is a direct approach to studying the optical characteristics and band structure of semiconductor materials. The optical transmittance (*T*) and absorption (*Abs*) spectra of ZnO NWs fabricated on glass substrates with different impurity ratios are

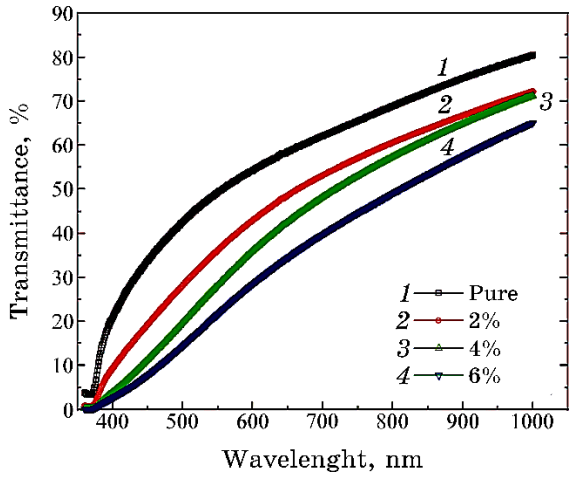

Fig. 1. Optical transmittance spectra of ZnO NWs prepared with different doping ratios.

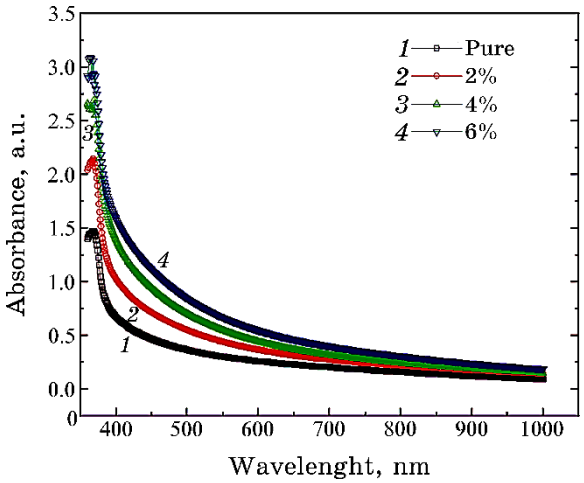

Fig. 2. Optical absorption spectra of ZnO NWs prepared with different doping ratios.

shown in Figs. 1, 2, respectively. These spectra show that the materials have low optical T in the visible range (400–700 nm). It was found that, as the impurity ratios grow from 0 to 6 wt.%, the transmittance values decrease, the absorption values increase, and the fundamental absorption edge shifts toward lower energies, or longer wavelengths. This may be due to the donor levels increasing near the conduction band [31].

Moreover, a decline in transmittance from 80% to 60% has been

noted in the visible region of the spectrum with a small transmittance in the ultraviolet region known as the absorption. As the aluminium-doping ratio increased, the absorption likewise increased from 1.5 to almost 3.5, and it is well known that this is one of the factors used to calculate several optical constants, including optical energy [32]. This indicates that the doping caused actual donor levels to form within the energy gap and close to the absorption edge. These donor levels then absorb low-energy photons, resulting in a noticeable increase in the absorption-coefficient values. Consequently, this allowed us to select the proper activation ratio, or the necessary sample to block the necessary portion of the solar spectrum in the context of solar cell manufacturing, for instance [33].

The absorption-coefficient values (α) for all prepared formulations were obtained using the Beer–Lambert law [34] according to the following equation:

$$\alpha\ [\mathrm{cm}^{-1}] = -\ln(T)/t\,, \tag{1}$$

where t is the thickness; the samples had a thickness of approximately 541 nm.

The optical energy gap of the prepared samples was calculated using Tauc's relation according to the following equation [35]:

$$\alpha h\nu = A\left(h\nu - E_g\right)^n, \tag{2}$$

where h is Planck's constant, ν is the frequency of the incident light photon, and A is a constant that depends on the values of the effective mass of the charge carriers; n depends on the nature of the prevailing optical transitions.

Figure 3 shows the α spectra of ZnO NWs grown on glass substrates with different impurity ratios. As shown in Fig. 3, the α of NWs in the UV region increased from $\cong 1.3 \cdot 10^5$ cm^{-1} to $\cong 6.0 \cdot 10^4$ cm^{-1} with the increase of impurity ratio. This behaviour can be attributed to the difference in impurity ratios.

Figure 4 shows the relationship between $(\alpha h\nu)^2$ and $h\nu$ for ZnO NWs doped with different doping ratios (0–6 wt.%), where they decreased optical energy gap $E_g = h\nu$ from 3.2 eV to 3.1 eV with increasing doping ratios, respectively. We also notice from Fig. 4 that the optical absorption edge showed a redshift. The decrease in the energy gap of the prepared samples with increasing doping ratio can be observed in Table 2 and Fig. 4, and can be attributed to the Burstein–Moss shift [36].

Thus, for ZnO NWs made on glass substrates (see Fig. 5), the development of different intensities of the (002) plane was ascribed to the crystallite-size variation and lattice-strain effects on the struc-

tural-parameters' current values.

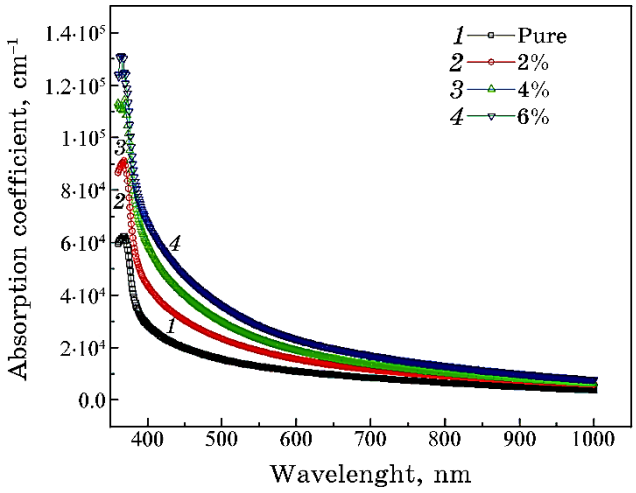

Fig. 3. Suggested malfunction spectra of ZnO NWs prepared with different doping ratios as the wavelength functions.

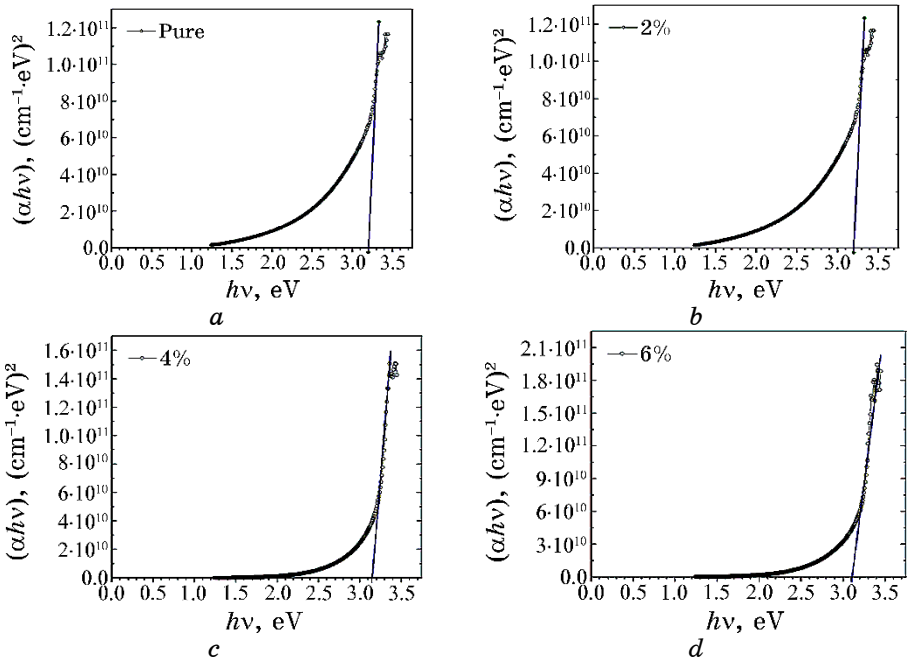

Fig. 4. The relationship between $(\alpha h\nu)^2$ and $h\nu$ for ZnO NWs prepared with different doping ratios.

TABLE 2. Experimental results of ZnO NWs synthesized on glass substrates with different doping ratios.

Doping rate, wt.%	E_g, eV	*FWHM*, degree	2θ, degree	*D*, nm	δ, nm^{-2}	ε, a.u.	*d*, nm	Lattice parameters	
								$a_{(100)}$, Å	$c_{(002)}$, Å
Pure	3.2	0.16398	34.4484	53.0	3.56E-04	0.002308	0.260138	3.2481	5.2027
2%	3.15	0.14381	34.4502	60.4	2.74E-04	0.002024	0.260125	3.2448	5.2025
4%	3.13	0.1595	34.4447	54.5	3.37E-04	0.002245	0.260166	3.2470	5.2033
6%	3.1	0.1552	34.4646	56.0	3.19E-04	0.002183	0.260020	3.2459	5.2003

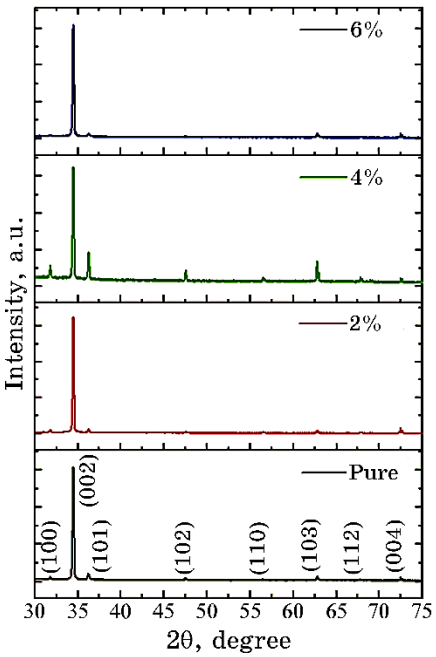

Fig. 5. XRD patterns of ZnO NWs prepared on glass substrates with different doping ratios.

Figure 5 shows that each peak can be matched with the standard pattern (JCPDS 36-1451). Each sample has a highly-crystalline wurtzite structure. The diffraction intensity of the ZnO NWs was significantly higher than that of the other axes, indicating that the NWs grew in line with the *c*-axis [37], which is because ZnO has the lowest surface free energy. In the 002 plane, no diffraction peaks of ZnO:Al NWs were observed in the XRD spectra, indicating that all samples had a preferential orientation of the *c*-axis perpendicular to the substrate surface. The intensity of the (002) peak of the ZnO:Al NWs is similar to that of the pure ZnO sample [38].

From the XRD patterns, the structural parameters including crystallite-size ratio (D), dislocation density (δ), lattice conformation (ε), interplanar distance (d), and lattice constants (a and c) of ZnO NWs were calculated using following equations [30]:

$$D = 0.94\lambda/(\beta\cos\theta)\,, \tag{3}$$

$$\delta = D^{-2}\,, \tag{4}$$

$$\varepsilon = \beta/(4\tan\theta)\,, \tag{5}$$

$$d = \lambda/(2\sin\theta)\,, \tag{6}$$

$$\frac{1}{d^2_{(hkl)}} = \frac{4}{3}\frac{h^2 + hk + k^2}{a^2} + \frac{l^2}{c^2}, \tag{7}$$

where the x-ray wavelength, Bragg's angle, Miller's indices of the crystal plane, and *FWHM* of the diffraction peak in radians are represented by the variables, λ, θ, *hkl*, and β, respectively. Table 2 contains a tabulation of all the calculated values.

The values of the structural parameters of the grown nanofibers differ slightly from those in previous studies [39, 40]. This divergence indicates that the values of the structural parameters were determined by the synthesis process and reaction parameters. We note that the increase in the crystal size in Table 2 and Fig. 5 with the increase in the doping ratio indicates an increase in the degree of crystallization of these samples after doping [41]. The crystal size of the samples prepared with different doping ratios was calculated based on the values of the (002) plane angle, which are ap-

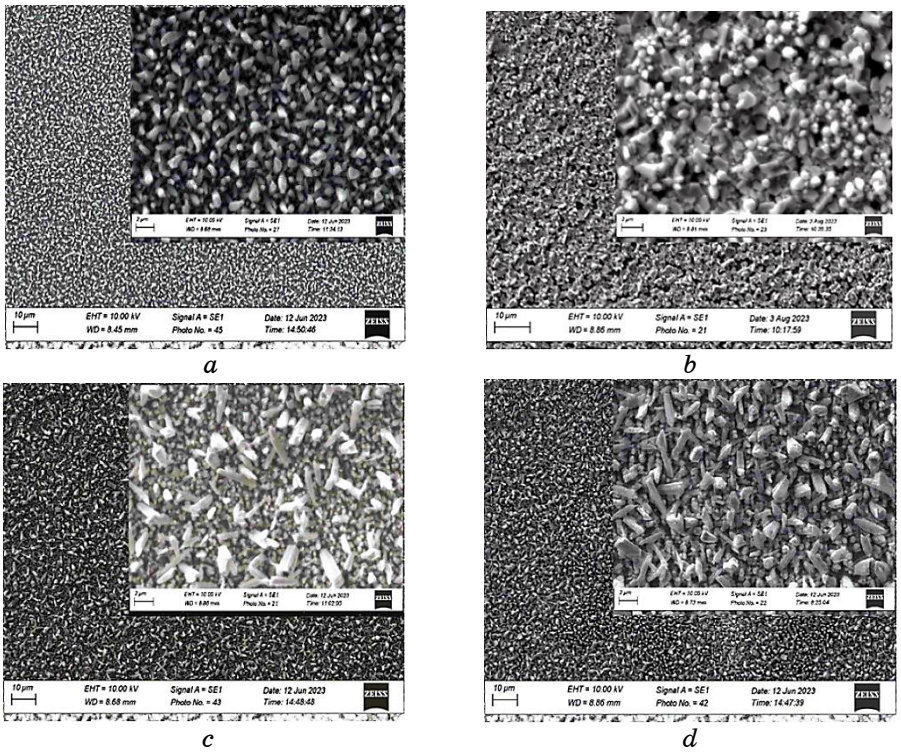

Fig. 6. SEM images of ZnO NWs grown with different doping ratios (*a*—0 wt.%, *b*—2 wt.%, *c*—4 wt.%, *d*—6 wt.%) on glass. The insets in *a*–*d* show a high-magnification top view of the grown ZnO NWs.

proximately equal to 34°, and the values were within the nanoscale. Table 2 shows samples prepared with a 2%-doping ratio, which has a low value of δ. This behaviour indicates a low defect rate in these samples [42].

Figure 6, *a*–*d* shows the FE–SEM images of the samples doped with aluminium with different ratios, where increasing the impurity content to 6% inhibited the growth process towards the *c*-axis, which has the lowest surface energy, indicating that the growth direction became more likely lateral (horizontal), leading to an increase in the diameter of the nanowires [43].

Using ImageJ 1.47v software, the average diameter ($D_{Avg.}$) of the grown nanowires was calculated from, at least, thirty measurements in FE–SEM images (see Fig. 6, *a*–*d*).

Figure 7 shows the distribution of the average diameters of the nanowires after the aluminium-doping process at different ratios (0, 2, 4, 6 wt.%); different diameters of ZnO NWs were obtained on

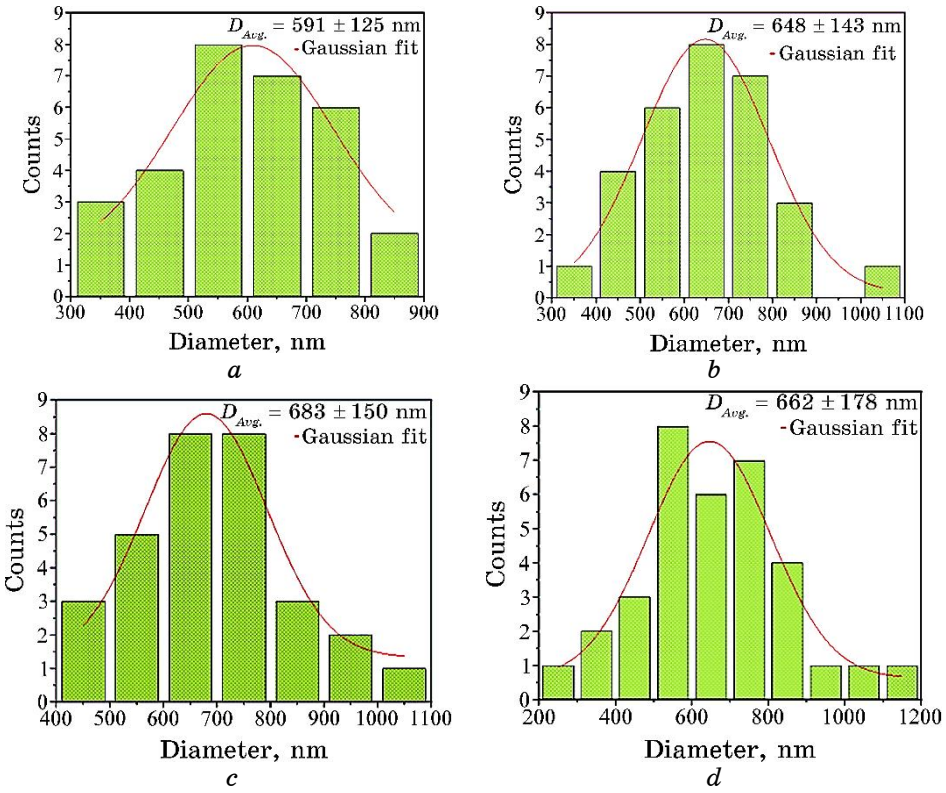

Fig. 7. Diameters' distribution for ZnO NWs prepared at different doping ratios: *a*—0%, *b*—2%, *c*—4%, and *d*—6%.

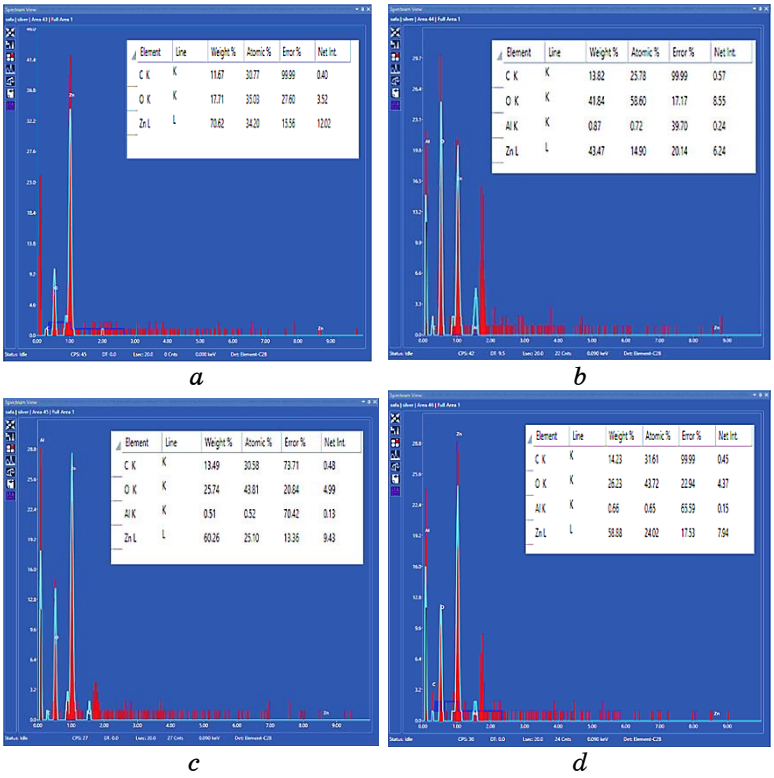

Fig. 8. EDX spectra of ZnO NWs prepared on glass substrates with different doping ratios.

glass substrates, and the average diameter increased from 591 ± 125 nm to 662 ± 178 nm as the doping ratio increases.

The growing-samples' diameters' distribution was fitted with a Gaussian distribution and shown as a solid red line in each histogram with the $D_{Avg.}$ serving as the peak position.

EDX analysis was performed as shown in Fig. 8 to evaluate the nanochemical composition of the samples grown on glass substrates, where the presence of carbon (C), oxygen (O), zinc (Zn), and aluminium (Al) elements was confirmed. EDX spectra clearly showed the doping material through this analysis, as its percentage increased significantly with increasing doping. This demonstrates that Al is integrated into the ZnO NWs [44].

4. CONCLUSION

ZnO NWs were successfully prepared on glass substrates using the

APCVD technique. The effect of changing the aluminium-impurity ratio on the physical properties of the synthesized samples was determined. Optical measurements revealed that the doped nanostructures resulted in decreased transmittance and increased absorption. This could be because the donor levels rise near the conduction band, and the absorption edge shifts to lower energies, which increases the probability of photon absorption. XRD results confirmed the synthesis of ZnO NWs with a hexagonal structure and a preferential orientation along the (002) lattice plane. FE–SEM images revealed the growth of ZnO NWs on glass substrates with different diameters, where the diameter of the nanowires increased with increasing the aluminium-doping ratio. EDX analysis confirmed the high purity of the synthesized samples. In addition, quantitative surface EDX results revealed that the zinc content with aluminium content was suitable for the doping ratios. Therefore, it was demonstrated that the addition of aluminium in different ratios plays a key role in improving the nanostructure properties and increasing the crystallinity of ZnO, using APCVD technique. Finally, our results demonstrate the potential of APCVD as a viable method for producing pure and doped ZnO nanowires.

ACKNOWLEDGMENTS

The authors acknowledge the support provided by the Iraqi Ministry of Higher Education and Scientific Research, as well as the University of Mosul for providing some financial assistance and for monitoring the status of the research.

REFERENCES

1. A. Shah, M. Ahmad, Rahmanuddin, Shakil Khan, Uzma Aziz, Zahid Ali, Afzal Khan, and A. Mahmood, *Applied Physics A*, **125**: Article No. 713 (2019); https://doi.org/10.1007/s00339-019-3005-y
2. R. Yousefi, *Doped ZnO Nanostructures: Growth Properties and Applications* (Eds. A. Umar) (American Scientific Publishers: 2011), vol. **2**, ch. 14, p. 1; doi:10.1039/C2JM15548F
3. R. S. Rai and V. Bajpai, *Adv. Nano Res.*, **11**, No. 1: 37 (2021); doi:10.12989/anr.2021.11.1.037
4. C. N. R. Rao, B. C. Satishkumar, A. Govindaraj, and Manashi Nath, *Nanotubes. ChemPhysChem*, **22**, Iss. 2: 78 (2001); https://doi.org/10.1002/1439-7641(20010216)2:2<78::AID-CPHC78>3.0.CO;2-7
5. S. Bagga, J. Akhtar, and S. Mishra, *AIP Conference Proceedings*, **1989**, No. 1: 020004 (2018); https://doi.org/10.1063/1.5047680
6. W. Z. Wang, B. Q. Zeng, J. Yang, B. Poudel, J. Y. Huang, M. J. Naughton, and Z. Ren, *Advanced Materials*, **18**, Iss. 24: 3275 (2006); https://doi.org/10.1002/adma.200601274

7. Bai Shouli, Chen Liangyuan, Li Dianqing, Yang Wensheng, Yang Pengcheng, Liu Zhiyong, Chen Aifan, and Chung Chiun Liu, *Sensors and Actuators B: Chemical*, **146**, Iss. 1: 129 (2010); https://doi.org/10.1016/j.snb.2010.02.011
8. Zhou Gui, Jian Liu, Zhengzhou Wang, Lei Song, Yuan Hu, Weicheng Fan, and Daoyong Chen, *The Journal of Physical Chemistry B*, **109**, Iss. 3: 1113 (2005); https://doi.org/10.1021/jp047088d
9. J. Q. Hu, Q. Li, X. Meng, C. Lee, and S. Lee, *Chemistry of Materials*, **15**, No. 1: 305 (2002); https://doi.org/10.1021/cm020649y
10. A. T. Ali, W. Maryam, Y. W. Huang, H. C. Hsu, N. M. Ahmed, N. Zainal, H. Abu Hassan, and M. A. Dheyab, *Journal of the Optical Society of America B*, **38**, No. 9: C69 (2021); https://doi.org/10.1364/JOSAB.427132
11. Oleg Lupan, Thierry Pauporté, Tangui Le Bahers, Bruno Viana, and Ilaria Ciofini, *Advanced Functional Materials*, **21**, Iss. 18: 3564 (2011); https://doi.org/10.1002/adfm.201100258
12. Yun-Ming Sung, Fang-Chi Hsu, and Yang-Fang Chen, *Solar Energy Materials and Solar Cells*, **125**: 239 (2014); https://doi.org/10.1016/j.solmat.2014.03.014
13. Te-Hua Fang and Shao-Hui Kang, *Current Nanoscience*, **6**, No. 5: 505 (2010); https://doi.org/10.2174/157341310797574961
14. Sang Kyoo Lim, Seong Hui Hong, Sung-Ho Hwang, Won Mi Choi, Soonhyun Kim, Hyunwoong Park, and Min Gi Jeong, *Journal of Materials Science & Technology*, **31**, Iss. 6: 639 (2015); https://doi.org/10.1016/j.jmst.2014.12.004
15. Jitesh Agrawal, Tejendra Dixit, I. A. Palani, and Vipul Singh, *IEEE Sensors Letters*, **3**, Iss. 9: 9900134 (2019); https://doi.org/10.1109/LSENS.2019.2938638
16. Pierre Gaffuri, Tatjana Dedova, Estelle Appert, Mati Danilson, Adrien Baillard, Odette Chaix-Pluchery, Frank Güell, Ilona Oja-Acik, and Vincent Consonni, *Applied Surface Science*, **582**: 152323 (2022); https://doi.org/10.1016/j.apsusc.2021.152323
17. Frank Maldonado and Arvids Stashans, *Journal of Physics and Chemistry of Solids*, **71**, Iss. 5: 784 (2010); https://doi.org/10.1016/j.jpcs.2010.02.001
18. Soaram Kim, Giwoong Nam, Hyunggil Park, Hyunsik Yoon, Sang-Heon Lee, Jin Soo Kim, Do Yeob Kim, Sung-O Kim, and Jae-Young Leem, *Bulletin of the Korean Chemical Society*, **34**, No. 4: 1205 (2013); https://doi.org/10.5012/bkcs.2013.34.4.1205
19. Ziling Peng, Dan Wu, Wei Wang, Fatang Tan, Xinyun Wang, Jianguo Chen, and Xueliang Qiao, *Powder Technology*, **315**: 73 (2017); https://doi.org/10.1016/j.powtec.2017.03.052
20. A. Nakrela, N. Benramdane, A. Bouzidi, Z. Kebbab, M. Medles, and C. Mathieu, *Results in Physics*, **6**: 133 (2016); https://doi.org/10.1016/j.rinp.2016.01.010
21. T. Holloway, R. Mundle, H. Dondapati, R. B. Konda, M. Bahoura, and A. K. Pradhan, *Proc. SPIE 8344. Nanosensors, Biosensors, and Info-Tech Sensors and Systems 2012 (30 March, 2012)*, **8344A**; https://doi.org/10.1117/12.914482
22. Sining Yun, Juneyoung Lee, Jahyun Yang, and Sangwoo Lim, *Physica B: Condensed Matter*, **405**, Iss. 1: 413 (2010);

https://doi.org/10.1016/j.physb.2009.08.297
23. Hua Zheng, Rong-Jun Zhang, Da-Hai Li, Xin Chen, Song-You Wang, Yu-Xiang Zheng, Meng-Jiao Li, Zhi-Gao Hu, Ning Dai, and Liang-Yao Chen, *Nanoscale Research Letters*, **13**: Article No. 149 (2018); https://doi.org/10.1186/s11671-018-2563-9
24. D. H. Zhang, Z. Y. Xue, and Q. P. Wang, *Journal of Physics D: Applied Physics*, **35**, Iss. 21: 2837 (2002); https://doi.org/10.1088/0022-3727/35/21/321
25. Jae Hyoung Choi, Hitoshi Tabata, and Tomoji Kawai, *Journal of Crystal Growth*, **226**, Iss. 4: 493 (2001); https://doi.org/10.1016/S0022-0248(01)01388-4
26. D. F. Paraguay, M. Miki-Yoshida, J. Morales, J. Solis, and W. Estrada L., *Thin Solid Films*, **373**, Nos. 1–2: 137 (2000); https://doi.org/10.1016/S0040-6090(00)01120-2
27. Jin Zhang and Wenxiu Que, *Solar Energy Materials and Solar Cells*, **94**, Iss. 12: 2181 (2010); https://doi.org/10.1016/j.solmat.2010.07.009
28. Mariana Fraga and Rodrigo Pessoa, *Micromachines*, **11**, No. 9: 799 (2020); https://doi.org/10.3390/mi11090799
29. Hong Jin Fan, Bodo Fuhrmann, Roland Scholz, Cameliu Himcinschi, Andreas Berger, Hartmut Leipner, Armin Dadgar, Alois Krost, Silke Christiansen, and Ulrich Gösele, *Nanotechnology*, **17**, No. 11: S231 (2006); doi:10.1088/0957-4484/17/11/S02
30. Iman Amer Ahmad and Yasir Hussein Mohammed, *Micro and Nanostructures*, **181**: 207628 (2023); https://doi.org/10.1016/j.micrna.2023.207628
31. Ilyass Jellal, Hassan Ahmoum, Yassine Khaaissa, Khalid Nouneh, Mourad Boughrara, Mounir Fahoume, Siddheshwar Chopra, and Jamal Naja, *Applied Physics A*, **125**: Article No. 650 (2019); https://doi.org/10.1007/s00339-019-2947-4
32. S. Ilican, Y. Caglar, and M. Caglar, *Journal of Optoelectronics and Advanced Materials*, **10**, No. 10: 2578 (2008); https://joam.inoe.ro/articles/preparation-and-characterization-of-zno-thin-films-deposited-by-sol-gel-spin-coating-method/fulltext
33. S. Kasap and P. Capper, *Springer Handbook of Electronic and Photonic Materials* (Eds. S. Kasap and P. Capper) (Springer International Publishing AG: 2017), vol. **1**, ch. 4, p. 723–1095; doi:10.10071978-3-319-48933-9
34. N. Yahya, *Carbon and Oxide Nanostructures* (Eds. N. Yahya) (New York–Berlin–Heidelberg: Springer: 2011), vol. **5**, ch. 3, p. 263–280; https://doi.org/10.1007/978-3-642-14673-2
35. S. Kasap, and P. Capper, *Springer Handbook of Electronic and Photonic Materials* (Eds. S. Kasap and P. Capper) (Springer International Publishing AG: 2017), vol. **1**, ch. 4, p. 723–1095; doi:10.10071978-3-319-48933-9
36. Haixia Chen, Jijun Ding, Wenge Guo, Feng Shi, and Yingfeng Li, *Applied Surface Science*, **258**, Iss. 24: 9913 (2012); https://doi.org/10.1016/j.apsusc.2012.06.050
37. L. D. Tang, B. Wang, J. G. Qi, S. J. Peng, and J. Z. Wang, *Materials Research Innovations*, **19**, Iss. 9: S9-6 (2015); https://doi.org/10.1179/1432891715Z.0000000001904
38. Y. Geng, L. Guo, S. S. Xu, Q. Q. Sun, S. J. Ding, H. L. Lu, and D. W. Zhang, *The Journal of Physical Chemistry C*, **115**, No. 25: 12317 (2011); https://doi.org/10.1021/jp2023567

39. Carina Hedrich, Stefanie Haugg, Leutrim Pacarizi, Kaline P. Furlan, Robert H. Blick, and Robert Zierold, *Coatings*, **91**, Iss. 1: 698 (2019); https://doi.org/10.3390/coatings9110698
40. S. Paiman, T. H. Ling, M. Husham, and S. Sagadevan, *Results in Physics*, **17**: 103185 (2020); https://doi.org/10.1016/j.rinp.2020.103185
41. L. Chabane, N. Zebbar, M. L. Zeggar, M. Aida, M. Kechouane, and M. Trari, *Materials Science in Semiconductor Processing*, **40**: 840 (2015); https://doi.org/10.1016/j.mssp.2015.07.080
42. T. Srinivasulu, K. Saritha, and K. T. Ramakrishna Reddy, *Modern Electronic Materials*, **3**, Iss. 2: 76 (2017); https://doi.org/10.1016/j.moem.2017.07.001
43. Mohammad R. Alenezi, Simon J. Henley, Neil G. Emerson, and S. Ravi P. Silva, *Nanoscale*, **6**, Iss. 1: 235 (2014); https://doi.org/10.1039/C3NR04519F
44. Gregor Zimmermann, Martin Lange, Bingqiang Cao, Michael Lorenz, and Marius Grundmann, *physica status solidi (RRL)–Rapid Research Letters*, **4**, Nos. 3–4: 82 (2010); https://doi.org/10.1002/pssr.201004015